applied sciences

MDPI

Article

Comparison of Different Numerical Methods in Modeling of Debris Flows—Case Study in Selanac (Serbia)

Jelka Krušić [1], Manuel Pastor [2], Saeid M. Tayyebi [2,*], Dragana Đurić [1], Tina Đurić [1], Mileva Samardžić-Petrović [3], Miloš Marjanović [1] and Biljana Abolmasov [1]

[1] Faculty of Mining and Geology, University of Belgrade, Djušina, 7, 11000 Belgrade, Serbia; jelka.krusic@rgf.bg.ac.rs (J.K.); dragana.djuric@rgf.bg.ac.rs (D.Đ.); tina.djuric@rgf.bg.ac.rs (T.Đ.); milos.marjanovic@rgf.bg.ac.rs (M.M.); biljana.abolmasov@rgf.bg.ac.rs (B.A.)
[2] Department of Applied Mathematics, ETS Ingenieros de Caminos, Universidad Politécnica de Madrid, Calle del Profesor Aranguren, 3, 28040 Madrid, Spain; manuel.pastor@upm.es
[3] Faculty of Civil Engineering, University of Belgrade, Bulevar Kralja Aleksandra 73, 11000 Belgrade, Serbia; mimas@grf.bg.ac.rs
* Correspondence: saeid.moussavita@upm.es

Abstract: Flow-type landslides are not typical in this region of the Balkans. However, after the Tamara cyclone event in 2014, numerous such occurrences have been observed in Serbia. This paper presents the initial results of a detailed investigation into debris flows in Serbia, comparing findings from two programs: RAMMS DBF and Geoflow SPH. Located in Western Serbia, the Selanac debris flow is a complex event characterized by significant depths in the initial block and entrainment zone. Previous field investigations utilized ERT surveys, supplemented by laboratory tests, to characterize material behavior. Approximately 450,000 m^3 of material began to flow following an extreme precipitation period, ultimately traveling 1.2 km to the deposition zone. For validation purposes, ERT profiles from both the deposition zone and the source area were utilized, with particular attention given to areas where entrainment was substantial, as this had a significant impact on the final models. The first objective of this research is to conduct a detailed investigation of debris flow using field investigations: geophysical (ERT) and aerial photogrammetry. The second objective is to evaluate the capacity of two debris flow propagation models to simulate the reality of these phenomena. The GeoFlow-SPH code overestimated the maximum propagation thickness in comparison to the RAMMS model. The numerical results regarding final depths closely align, especially when considering the estimated average depth in the deposition zone. The results confirm the necessity of using multiple simulation codes to more accurately predict specific events.

Keywords: Tamara cyclone; debris flow; entrainment; RAMMS; SPH; ERT

Citation: Krušić, J.; Pastor, M.; Tayyebi, S.M.; Đurić, D.; Đurić, T.; Samardžić-Petrović, M.; Marjanović, M.; Abolmasov, B. Comparison of Different Numerical Methods in Modeling of Debris Flows—Case Study in Selanac (Serbia). *Appl. Sci.* **2024**, *14*, 9059. https://doi.org/10.3390/app14199059

Academic Editor: Haiqing Yang

Received: 9 August 2024
Revised: 17 September 2024
Accepted: 26 September 2024
Published: 8 October 2024

1. Introduction

Debris flows are characterized as one of the most dangerous and least predictable types of landslides [1,2]. Following certain natural disasters, flow-type landslides frequently occur. In Serbia, numerous such events occurred in 2014 due to the Tamara cyclone effect. Specifically, over 200 flow-type landslides were recorded in the western part of Serbia, with many others identified indirectly through satellite image analysis [3,4]. Many of these incidents were unexpected, even in areas designated as relatively stable according to hazard maps. Some cases were particularly complex, involving both sliding and flowing processes and a significant volume of material, rendering them challenging for numerical modeling.

Various runout methods have been developed over time, ranging from empirical relationships between runout and landslide initial characteristics [5], to analytical methods [1,6–8], and finally to dynamic and complex numerical methods [9–11]. The complexity of modeling lies in the consideration of numerous input parameters, including the appropriate rheology law, accurate depth of the source area, entrainment parameters, and

the definition of geotechnical parameters such as porosity, friction coefficients, and the variation in pore water pressure over time and space [12,13].

Some software is designed for ease of use but is also continuously developed and improved to enhance numerical capabilities in line with the needs and complexity of real-world scenarios. In cases involving large deformations, large-scale phenomena, and hazard prediction, propagation models (runout models) have proven to be highly effective. After identifying unstable areas where mass flows are likely to occur, current programs utilizing dynamic numerical models are used to predict flow patterns and pinpoint potential impact zones. Today, numerous numerical models are available for risk assessment and runout analysis, and selecting the most appropriate simulation code has become a significant concern due to advances in computational technology.

Running multiple simulations to predict specific events or conducting a detailed back-analysis can be valuable. This approach enables a comparison of numerical outcomes, helps identify key differences, and allows for a more precise assessment of potential risks. However, beyond the capabilities of the chosen simulation code, various other factors—such as the presence of erosion and the accurate definition of parameters—can greatly influence the results.

RAMMS is widely utilized for back-calculating models of avalanches and debris flows. Its inclusion of entrainment calculation has been thoroughly tested in study areas [14]. The model operates in 2D, tracking the changing volume over time using Voellmy rheology, a method commonly employed in debris flow modeling. The initial models for this study area were developed using RAMMS, facilitating the straightforward determination of certain input parameters. This involved utilizing terrain data with a resolution of 5×5 m (presented here are the final models based on this resolution DTM) and identifying zones of potential maximum erosion depth. For accurate interpretation, detailed field characterization of the cases being modeled was essential. These study areas were delineated through various field research methods: Electrical Resistivity Tomography (ERT), detailed UAV scanning of the wider area to generate post-event orthophotos, and a DTM with a 5 cm resolution. Additionally, laboratory tests were conducted to analyze granulometry and consistency across different samples.

SPH (Smoothed Particle Hydrodynamics) is a meshless method utilized across various fields. Geoflow SPH, proposed by [10], has been implemented and tested over the years on numerous cases [10,15,16], including different scenarios and flume tests. For the first time in this study, the extraction of the source area from the topographical model was employed to enhance the accuracy of entrainment calculation. Also, many other researchers have developed this SPH model [17–20]. Here, we present a two-phase model that includes entrainment calculation.

Conducting detailed geotechnical investigations is crucial for acquiring field data. Given the extensive scale of this study area, traditional geotechnical methods such as drilling may not be feasible. Electrical Resistivity Tomography (ERT) geophysical research was therefore employed to effectively delineate key dimensional parameters of the debris flow, including depth in the source area, potential erosion depths, and depths in the deposition zone. Since the 2000s, numerous papers have reported the successful application of geophysical methods in landslide investigations, enabling the determination of various parameters such as the thickness of alluvial deposits, depth of bedrock, and shear surfaces [21,22]. Among these methods, Electrical Resistivity Tomography (ERT) stands out as particularly useful for landslide investigations [23,24]. Additionally, comparing precise satellite images from different epochs serves as a valuable system for validating final models.

This paper is structured as follows: the second section is divided into study area characteristics, geology conditions of the field, investigation methods, and numerical methods. Finally, in the results section, the final propagation models in both programs are shown with a validation using the ERT deposition profile.

2. Materials and Methods

2.1. Study Area

The Selanac debris flow was triggered by an extreme precipitation period in May 2014. Following a month of nearly continuous rainfall, floods inundated a vast area of Serbia, triggering numerous new landslides, some of which were reactivated occurrences. Consequently, many of these events took place unexpectedly in areas where such incidents were not anticipated, with most being characterized as flow-type landslides or involving combined processes [25]. Western Serbia bore the brunt of the impact, with over 200 flow-type landslides recorded in the field. The Selanac debris flow is situated in the northern part of the Ljubovija municipality (Figure 1) and garnered significant attention due to its behavior and magnitude (involving 450,000 m^3 of triggered material). The massive block of material initially slid in the upper part, and then transitioned into a flow through two existing gullies. It is noteworthy that a smaller event occurred first in the upper part, although it was part of a separate landslide. The transported material descended to an elevation approximately 320 m lower, depositing a heterogeneous mix ranging from matrix to huge boulders up to 2 m in diameter. Initially, the material formed a dam on the Selanačka river, which was subsequently breached by the torrential flow of the Selanačka river, leading to the further transportation of material down the river valley and causing instabilities. This paper focuses on the model for the initial deposition area, while all other materials are regarded as outflow material.

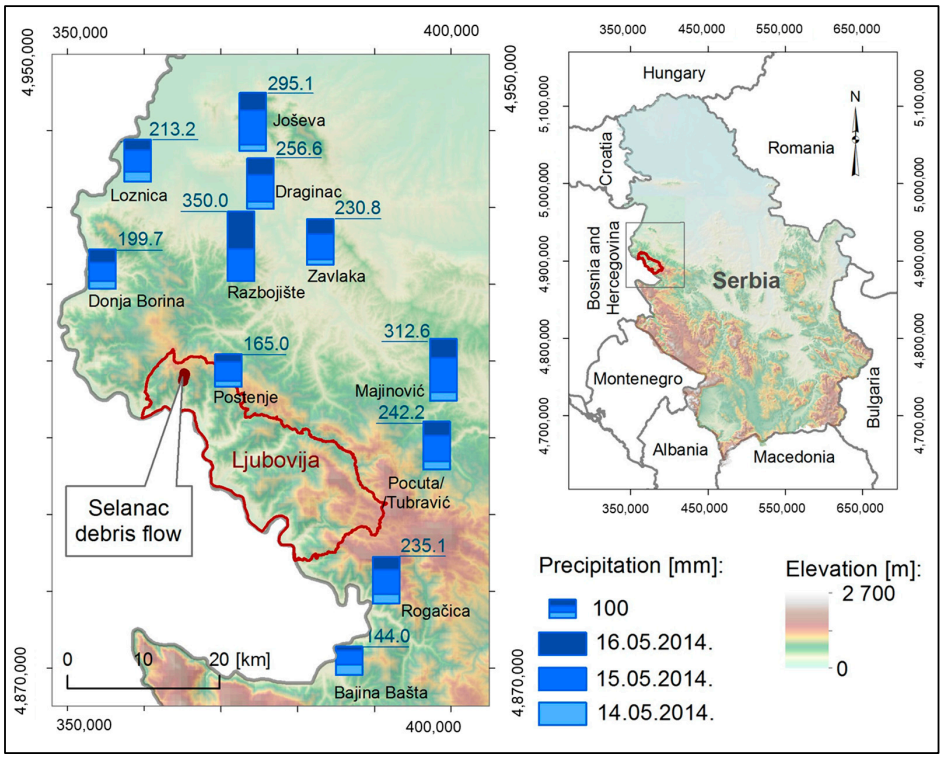

Figure 1. Location of the study area with measured precipitation amounts at the nearest weather stations.

The study area is located in the municipality of Ljubovija, specifically in the Selanac region. The broader area is characterized by a moderately continental to continental climate. The Ljubovija region is situated on the right valley side of the Drina River and is marked by steep slopes prone to instability, including erosion, sliding, flow, and flooding. In addition to the Drina River, one of the major watercourses in the area is the Ljubovića River, which exhibits a pronounced torrential characteristic. The elevation in the broader study area ranges from 158 m in the lower parts of the Drina River valley to 1268 m in the mountainous regions. The terrain is generally mountainous to hilly. Within the flow

activation zone, the initial zone is located at approximately 720 m above sea level, while the material deposition zone is at an elevation of about 400 m above sea level, extending down to the Selanačka River.

During this period, there was heavy rainfall for three days. In Western Serbia, the maximum recorded rainfall was 350 mm, which was measured at Razbojište, one of the nearest measurement stations to the Selanac debris flow (Figure 1).

2.2. Geology Conditions

There are two dominant geological formations in the wider area: the 'Drina' formation and the 'Jadar' formation. The 'Drina' formation comprises a complex of Lower- ($^{1}C_{1,2}$) and Middle-Carboniferous-age ($^{2}C_{1,2}$) phyllite, metasandstone, clay and graphitic schists, limestone, diabase, tuff, and tuffite. The 'Jadar' formation (Pz) consists of a complex of sandstone, argillophyllite, and black limestone. These formations overlay transgressively above Permian sediments of shales, sandstones, and limestones, with the limestones transitioning into a block of Upper Permian bituminous limestone. The primary geological unit involved in the debris flow process is the ophiolitic melange of the Jurassic period. It is believed that huge boulders of rock were mixed within a matrix mass. In the upper part, just a few hundred meters from the source area, lies the fault zone with limestones. Other units include Jurassic limestones and Triassic limestones in the middle part. In the zone of the deposition area, magmatic rocks such as granodiorite, dacite, andesite, quartz-latite, and basalt formed during the Tertiary period (Tc) (Figure 2).

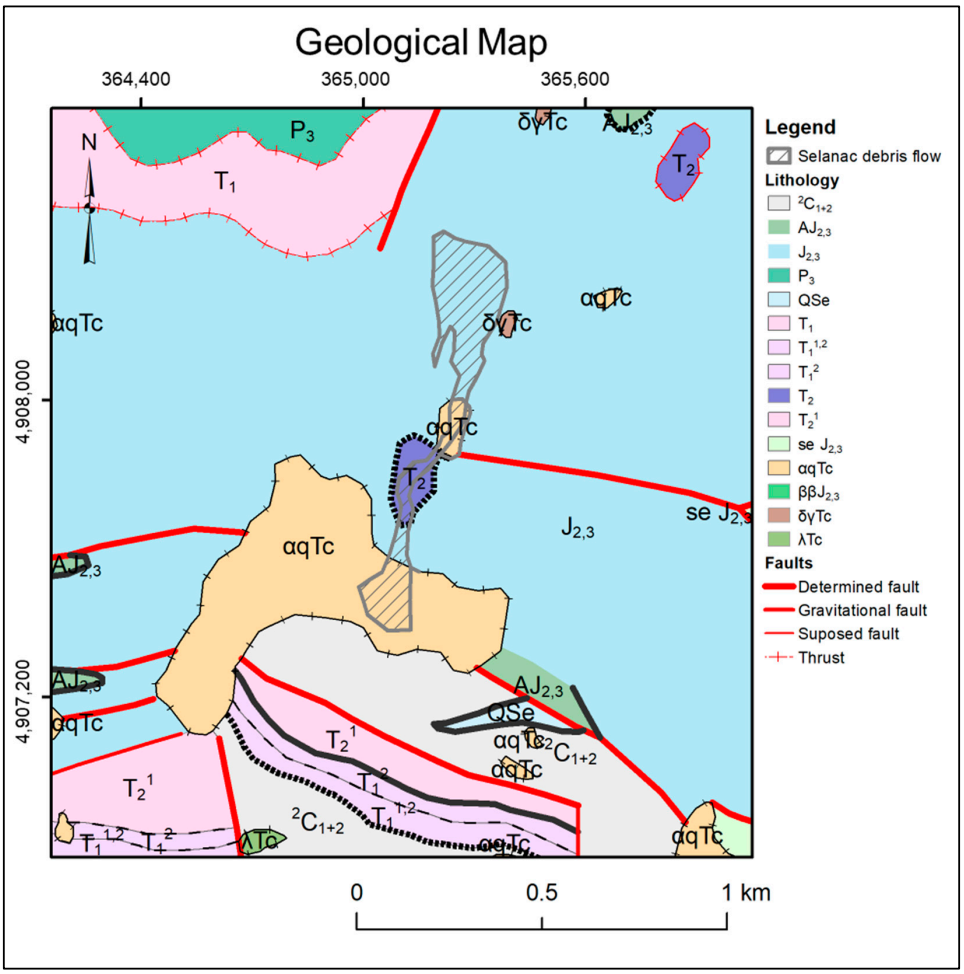

Figure 2. Geological map of the terrain, detailed at 1:10,000 of the general geological map (OGK) at 1:100,000, Ljubovija.

2.3. Investigation

The first field survey was conducted in May 2015 to document the phenomena that occurred following the impact of cyclone Tamara in 2014, as part of the BEWARE project. During this survey, the basic geometric characteristics of the debris flow were defined, including its length, potential depth, the material transport zone with an estimated depth, rock mapping, and the characterization of displaced blocks.

After mapping the terrain, sampling for laboratory tests was conducted. Samples were collected from the initiation zone, transportation zone, and deposition zone. The material in the debris flow is highly heterogeneous and transported over long distances, with the majority of the coarse material accumulating in the deposition zone. Since these are "disturbed" samples, soil samples were taken to be representative for laboratory analysis. In selecting the samples, care was taken to ensure representation from each element of the flow. Six samples were selected for laboratory testing: 3 from the initiation zone, 2 from the deposition zone, and 1 from the transportation zone.

Due to the inaccessibility of the terrain and the significant depth of the debris flow, it was not possible to apply classical geotechnical methods to define the thickness of the mobilized and transported material. In November 2015, geophysical investigations using the Electrical Resistivity Tomography (ERT) method were conducted to precisely characterize the geometry of the debris flow and compare it with subsequent numerical analyses. In March 2017, photogrammetric imaging was performed to compare images before and after the activation of the flow, and to analyze the resulting Digital Terrain Model (DTM) and high-resolution orthophoto images (with up to 10 cm accuracy). The DTM of the terrain prior to the flow activation was obtained by restituting high-resolution aerial images and was used as input data in flow modeling software.

2.3.1. Remote Detection Methods

Remote sensing methods were employed during the investigation to promptly assess the aftermath of cyclone Tamara as part of the project. The Pleiades satellite image for Selanac from June 2014 was scrutinized, taken immediately after the landslide activation in May 2014. This satellite image served visualization purposes and facilitated the determination of the location and extent of the broader investigation area [4]. Subsequently, other remote sensing methods were utilized to primarily gather more precise data, such as generating a high-resolution Digital Terrain Model (DTM). In landslide modeling, we can consider two epochs crucial for analyzing the distribution of moved material due to instability:

Epoch I: Referring to the stable terrain before the activation of the landslide;
Epoch II: Referring to the terrain after the activation of the landslide.

In order to obtain high-resolution orthophoto images and the DTM for the second epoch, after the activation of the flow, a DJI Phantom 4 Pro drone was used.

The procedure for capturing and creating the DTM and orthophoto images was carried out in the following order: the study areas and the desired pixel resolution of the orthophoto images were defined; flight parameters (altitude, flight path, and waypoint locations) were calculated, and the necessary percentages of longitudinal and lateral image overlap were determined; orientation points on the terrain surface were defined, marked, and surveyed; control points on the terrain surface were defined, marked, and surveyed; drone flights were conducted; the collected images were processed photogrammetrically; point clouds were classified, terrain surfaces were derived, and DTM and orthophoto images were created.

Comparing the DTMs of these epochs for both landslides served as a validation method for the final numerical models. The following figure (Figure 3) shows a high-resolution orthophoto of the large flow area where detailed field investigations and modeling were conducted. In addition to the defined elements, images of characteristic parts of the terrain are presented.

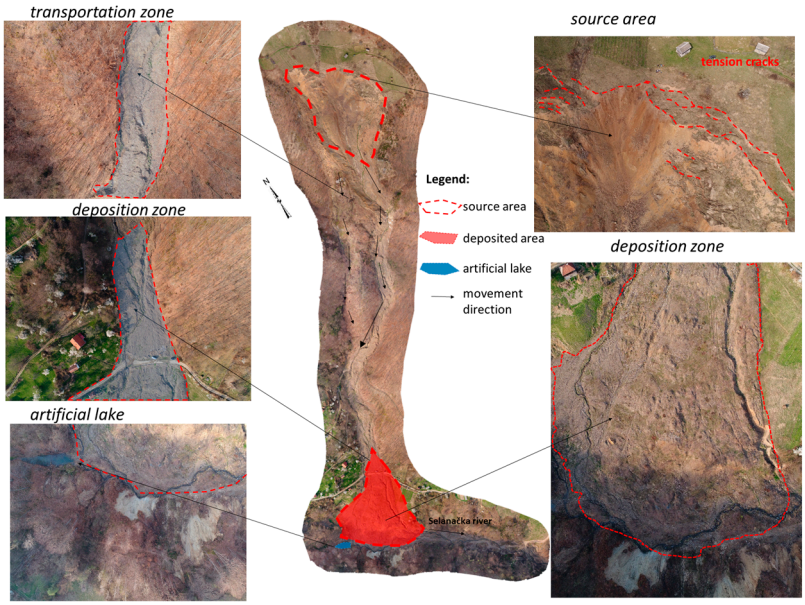

Figure 3. Orthophoto of the Selanac debris flow obtained by UAV photogrammetric survey with characterization of basic geometric elements.

To compare Digital Terrain Models from two epochs, the initial step involved resampling the model with a resolution of 30x30 cm to match the 5 m resolution used in the final modeling. To achieve a more precise comparison and obtain accurate data on mass differences before and after the activation of the debris flow, the scans from the two epochs overlapped (Figure 4). This overlap revealed the differences in terrain elevation within the debris flow zone.

The image clearly shows that in the initial zone, the maximum depth reaches nearly 29 m, while in the deposition zone, differences of up to 31 m are recorded. Additionally, in the transportation zone, there is a noticeable area of significant erosion along the right gully (red zone), as well as material deposition in the left gully (green zone). It should be noted that, due to the nature of the processes involved, these differences are most representative in the initial zone, where material transport was the dominant process. In the deposition zone, the reported values indicate precise differences (with the deepest values corresponding to the Selanac river bed). However, since both material transport and deposition occurred in this area, the exact depth of the deposited material cannot be determined with certainty from these data. This is especially relevant for the transportation zone, where both significant erosion and continuous material deposition are dominant.

The eroded and initiation zones were directly defined based on the results obtained from aerial photogrammetry (Figure 4). The red area in the initiation zone was identified as the initial block, while the red area in the transport zone was designated as the entrainment zone in both models. As noted, the two programs use different numerical approaches for calculating the eroded material.

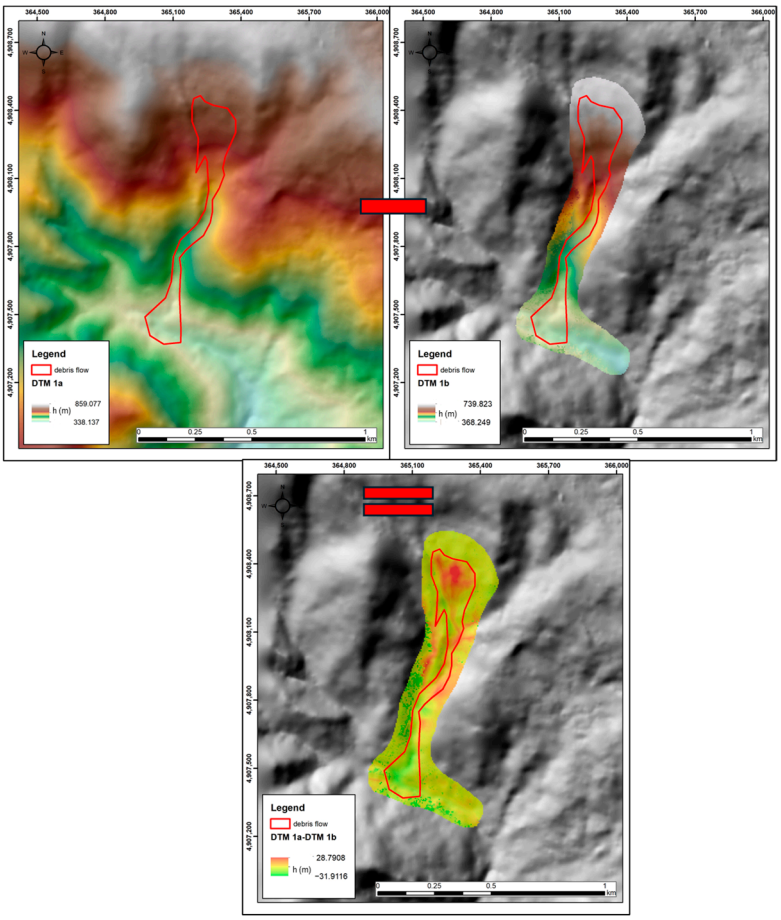

Figure 4. Map obtained by overlapping two epochs of the Digital Terrain Model (DTM).

2.3.2. Electrical Resistivity Tomography (ERT)

Electrical Resistivity Tomography (ERT) is a widely utilized method in geophysics, relying on the transmission of current through electrodes positioned along defined profiles. It correlates measured resistivity with various geological characteristics of the terrain, such as lithology, structural arrangement, moisture content, and water presence [21–24].

At the Selanac landslide site, ERT was employed to ascertain its geometric features, including the depth of the initial block, eroded and deposited material, and accumulated debris. Given the occurrence's dimensions, material heterogeneity, and the terrain's inaccessibility, traditional geotechnical investigation methods were impractical, making ERT the most suitable option. Measurements across all profiles were conducted using a '4-point light HP resistivity meter' (LGM Lippmann-GERMANY) with 20–60 electrodes. This system reduces the measurement time. All operational electrodes along the profile were connected to the resistivity meter via multi-core cables. For each individual measurement, the resistivity meter selects four electrodes and measures the apparent resistivity [22]. This research was conducted in November 2015 by the expert team from the Faculty of Mining and Geology, Department of Geophysics.

Validation was conducted by comparing a single cross-section corresponding to the position of the ERT5 profile in the deposition zone, as well as the difference in DTM heights. ERT5 (Figure 5) is located in the deposition zone of the transported material. It was not possible to determine the lateral boundaries, but the thickness of the accumulated material was estimated. For ERT5, the maximum thickness was estimated at 15–20 m(Figure 6).

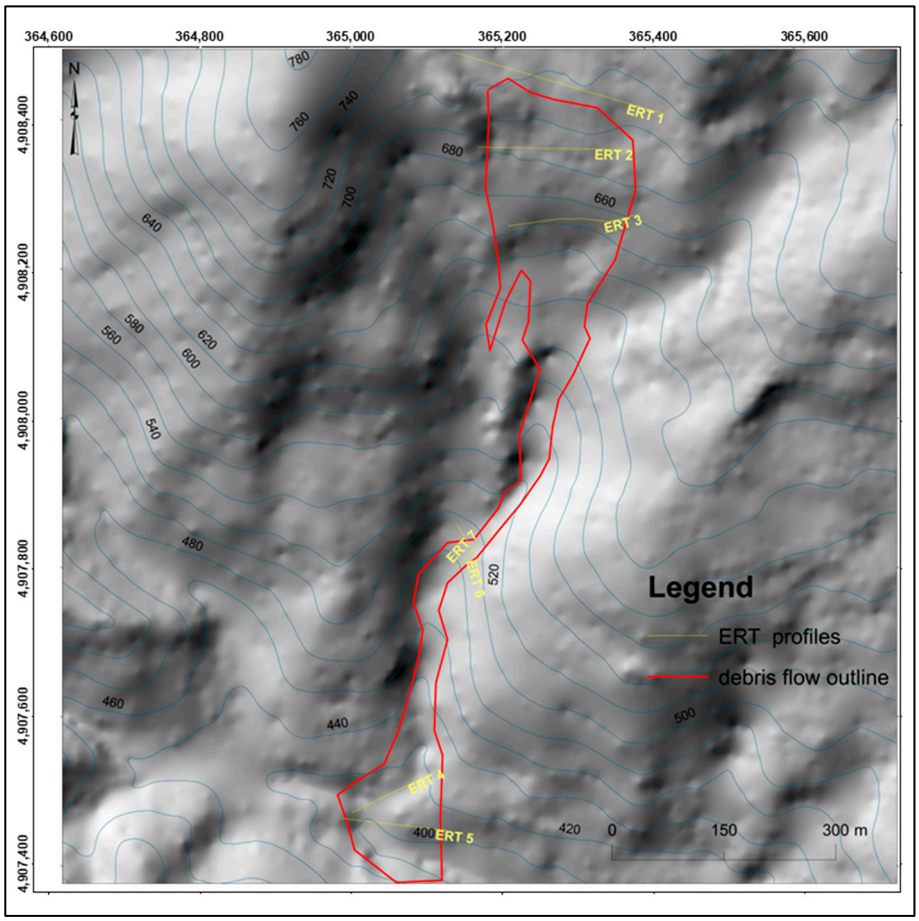

Figure 5. Position of the ERT profiles on the Digital Terrain Model.

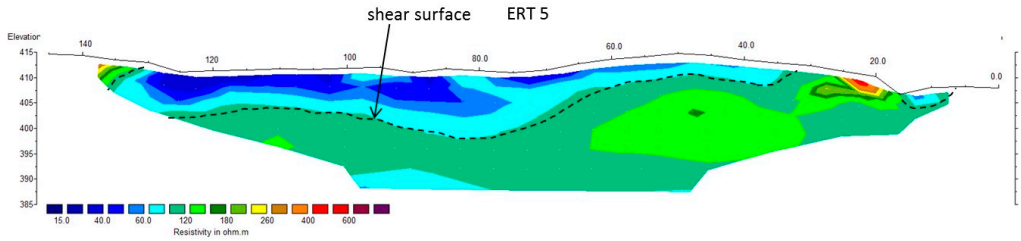

Figure 6. Results of ERT profile 5.

2.3.3. Laboratory Testing

Laboratory testing was conducted to define the basic identification and classification characteristics of the displaced material. Samples were collected from multiple locations of the landslide, excluding the deposition zone where the largest material was deposited. Given the significance of fine-grained material in defining landslide movements, care was taken in selecting samples to ensure the representation of fine particles, which are integral to the fluid.

The laboratory tests included sieving of the material, separation of the fine fraction for hydrometer analysis, selection of a portion of the fine fraction for determining specific gravity, and tests for plasticity and the falling cone test. To classify the landslide based on its grain size composition, laboratory tests for determining particle size distribution and hydrometer analysis were performed. The falling cone test, conducted to determine the flow limit, followed the standard SRPS EN ISO 17892-12 [26].

A sample prepared by adding water is placed in a vessel with a diameter of 55 mm. Each subsequent measurement is performed on the same sample with additional water

added. The values of cone penetration are read on the scale, and based on the recorded values, the flow limit value is obtained. Three measurements are taken on each sample.

For the classification of the mobilized material, the obtained samples are presented on the USCS diagram (Figure 7). The results show that the matrix has low to medium plasticity. Two samples, S1 taken from the initial zone and S4 from the deposition zone, are in the low-plasticity zone CL and on the border with the medium-plasticity state CL, while the other samples are characterized as clayey material of medium-plasticity CI. The results are within approximate limits and, considering the heterogeneous nature of the material and the large dimensions of the flow, they show a very good correlation when comparing the mobilized material in different elements of the flow.

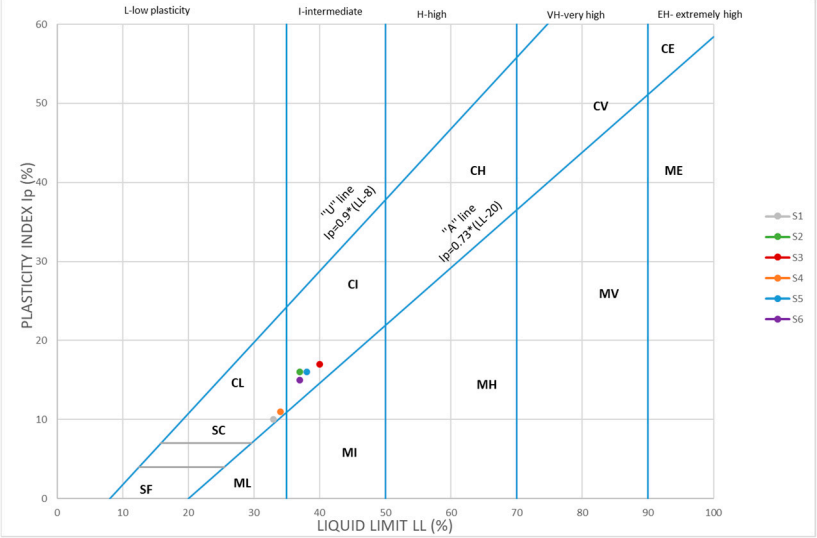

Figure 7. USCS diagram based on soil consistency parameters.

The plasticity test was conducted on selected samples by the Casagrande test, while the cone penetration test was conducted to determine the liquidity index, both according to the standard SRPS EN ISO 17892-12.

The consistency index (Ic) indicates the consistency (hardness) of the soil. As seen in Table 1, the Ic values range from −0.7 to 0. A negative value of the index indicates that the soil is in a liquid state. The natural moisture content of all samples was assumed to be 40%, as it was not possible to measure it in the field (samples were taken 3 years later), and the material behaved like a fluid. The obtained results for soil consistency and the determination of Atterberg consistency limits are presented in Table 1.

Table 1. Soil consistency parameters.

Samples	S1	S2	S3	S4	S5	S6
w (%)	40.0	40.0	40.0	40.0	40.0	40.0
LL (%)	33	37	40	34	38	37
PL (%)	23	21	23	23	22	22
I_p (%)	10	16	17	11	16	15
I_c (-)	−0.700	−0.188	0.000	−0.545	−0.125	−0.200

According to the established experiment, the specific weight of a sample with a mass of 49.73 g was determined. Based on this value, the density of solid particles was used as one of the input parameters in the SPH Geoflow modeling program. The results are presented in Table 2.

Table 2. Measurement results from the experiment determining the specific weight of sample St1.

Determination of Specific Weight of a Sample St1	
ms (g)	49.738
mpvm (g)	362.144
mpv (g)	331.554
Gs	2.60

2.4. Numerical Methods

Two different approaches were used for modeling landslide propagation in this research: one based on the Finite Volume Method (FVM) and the other based on the meshless Smoothed Particle Hydrodynamics (SPH) method. The first approach was implemented using the RAMMS DBF software, v. 1.5.0 while the second was implemented using code developed by the research group in Madrid [10].

In propagation modeling, the mathematical formulations used in simulations are often simplified and reduced to two dimensions through depth-integration approximations. Many flow-like landslides are relatively long and wide compared to their depth, allowing the governing equations to be integrated along the vertical axis. This 2D depth-integrated approach strikes a good balance between accuracy and computational efficiency. Models like RAMMS DBF and Geoflow SPH rely on integrated solutions of the mass and momentum balance equations, based on the shallow water flow assumption. While depth-integrated models provide valuable insights into landslide behavior, they have notable limitations due to their simplified representation of 3D dynamics, complex material properties, and terrain interactions. As a result, they are less effective for irregular terrains, complex flow behaviors, or when small-scale processes are important. However, these models are particularly useful for large-scale, shallow landslides and long-runout events, such as the Selanac debris flow. Overall, depth-integrated models offer a practical balance of simplicity, efficiency, and accuracy, making them highly valuable for landslide propagation studies.

2.4.1. RAMMS

RAMMS (Rapid Mass Movement Software) was specially developed (2005) from experts of Avalanche Research SLF and WSL Institute for Snow. The main development was made by researching a case study of Illgraben debris flow in Switzerland [14,27,28]. It is one-phase FVM (Finite Volume Method)-based, calculating displacement in a change in volume, pressure, and depth in time F(V, P, h, t).

As the main input data, the DTM (Digital Terrain Model) was used as information of terrain using automatic extraction of the source material. The suggested resolution was from 5 m to 25 m. Here, a pre-event DTM was used on 5 m. The calculation was carried out in a Cartesian coordinate system.

The mass balance equation incorporates the field variables flow height H (x, y, t) and flow velocity U (x, y, t) and is given by

$$Q(x,y,t)^{\cdot} = \partial tH + \partial x\ (H\ Ux) + \partial y\ (H\ Uy) \quad (1)$$

where the earth pressure coefficient ka = p is normally set to 1 when running the standard Voellmy–Salm friction approach, cx and cy represent topographical coefficients determined from the digital elevation model, Sg is the effective gravitational acceleration, and S_f is the frictional deceleration in directions x and y [28].

The frictional deceleration S_f of the flow is determined using the Voellmy friction relation and specifies the dry-Coulomb term (friction coefficient μ) scaling with the normal stress and the viscous or turbulent friction (coefficient ξ depending on the flow velocity U [11,29]:

$$S_f = \mu\rho gH\cos\varphi + \left(\rho g u^2\right)/\xi \quad (2)$$

where ρ is the mass density, g is the gravitational acceleration, φ is the slope angle, and Hgcos φ is the normal stress on the overflowed surface. The tangent of the effective internal friction angle of the flow material can be defined for the resistance of the solid phase (the term containing μ which extensively controls the deceleration behavior of a more slowly moving flow). The resistance of the viscous or turbulent fluid phase (the term including ξ) prevails for a more quickly moving flow [29].

Entrainment Model

The erosion algorithm in the RAMMS model is defined using the maximum potential erosion depth *em* and a specific erosion rate. The erosion algorithm predicts the maximum potential depth of erosion *em* as a function of the computed basal shear stress in each grid cell:

$$em = 0 \; for \; \tau < \tau c \tag{3}$$

$$em = \; dz/d\tau \; (\tau - \tau c) \text{for} \tau \geq \tau c \tag{4}$$

and the shear stress τ is approximated using the depth–slope product:

$$\tau = \rho g h S \tag{5}$$

The potential erosion depth (per kPa) dz/dt controls the rate of vertical erosion (in the z-direction) as a linear function of channel-bed shear stress.

When the critical shear stress τc is exceeded, sediment can be entrained from the channel. Entrainment stops when the actual erosion depth *et* reaches the maximum potential erosion depth *em* (Equation (6)). Normally, the specific erosion rate is implemented using the default value $dz/dt = -0.025$ m^{-1}.

2.4.2. SPH-Smoothed Particle Hydrodynamics

In this section, we perform the GeoFlow-SPH simulation model which has been developed in Madrid by an expert research team for almost a decade. It has previously been applied to theoretical, experimental, and real case histories.

First, we briefly describe a Lagrangian meshless numerical method of Smoothed Particle Hydrodynamics (SPH) that is used to transform the problems that are basically in the form of partial differential equations (PDEs) to a form suitable for particle-based simulation. The SPH method was first invented by [30,31] to model astrophysical problems. This technique has been applied in many areas due to its capability to model complicated cases that involve large-displacement deformations, such as modeling fast landslides in Solid Mechanics [32–34]. Good reviews can be found in the texts of [35,36].

In this model, these 3D problems are transformed into a 2D form by applying a depth-integrated model. As a result, the depth-integrated model provides an excellent combination of accuracy and computational time. This technique has been successfully applied to landslides by [15,16,37–41].

The two-phase depth-integrated SPH model we follow here is proposed based on the mathematical model proposed by Zienkiewicz and Shiomi [42] and is similar to those of [42–44].

To discretize the propagating mass in the SPH method, the first step is to present them as a set of nodes, as depicted in Figure 8, exhibiting individual material properties.

Then, an interpolation process calculates the relevant properties on each node over neighboring nodes through a kernel function $\left(W_{ij} = W\left(x_i - x_j, h\right)\right)$, without having to define any element. The formulation can be expressed as

$$f(x_i) = \int f(x_j) W(x_i - x_j, h) dx_j \tag{6}$$

where the function $f(x)$ is approximated at a position vector x in space.

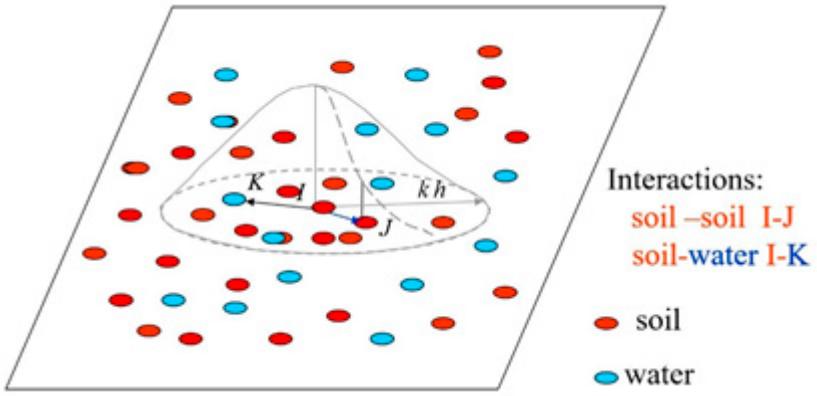

Figure 8. SPH interactions for two-phase model.

By applying the particle approximation technique and considering that the infinitesimal volume (dx_j) is related to the mass and density of the particle j, the function at particle i can be written as

$$f(x_i) \cong \sum_{j=1}^{N} f(x_j)(x_i - x_j, h)\frac{m_j}{\rho_j} \tag{7}$$

Then, in the numerical SPH method, the ordinary differential equations (ODEs) of the balance of mass and momentum can be produced in discretized form with respect to, respectively,

$$\frac{\overline{d}h_i}{dt} + h_i \sum_{j=1}^{Nh} \frac{m_j}{\rho_j} v_j \mathrm{grad}W_{ij} = \overline{n}_i e_R \tag{8}$$

$$\begin{aligned} \frac{\overline{d}^{(\alpha)}\overline{v}_{ai}}{dt} = -\sum_{j=1}^{Nh} m_{aj}\left(\frac{\overline{P}_{ai}}{h_{ai}^2} + \frac{\overline{P}_{aj}}{h_{aj}^2}\right)\mathrm{grad}W_{ij} - \left(\frac{1}{2}\frac{\rho_w}{\rho_\alpha}b_3 h_{ai}^2 - \frac{\Delta\overline{p}_w h_{ai}}{\rho_\alpha}\right)\sum_{j=1}^{Nh} m_{aj} \\ \left(\frac{\overline{n}_{ai}}{h_{ai}^2} + \frac{\overline{n}_{aj}}{h_{aj}^2}\right)\mathrm{grad}W_{ij} + \frac{1}{\rho_\alpha h_{ai}}\tau_B^{(\alpha)} + b_i + \frac{1}{\rho_\alpha}\overline{R}_\alpha - \frac{1}{h_{ai}}\overline{v}_{ai}\overline{n}_{ai}e_R \end{aligned} \tag{9}$$

where α denotes the phase (s or w), $\overline{n}_\alpha$ are the volume fractions of solid and fluid phases ($\overline{n}_s = 1 - \overline{n}$ and $\overline{n}_w = \overline{n}$), and $h_\alpha = h\overline{n}_\alpha$. $\overline{P}_\alpha$ is the averaged pressure $(\overline{P}_\alpha)$ acting on solid or fluid phases and can be defined as

$$\overline{P}_s = \frac{1}{2}b_3 h h_s + \frac{\Delta\overline{p}_w h\overline{n}}{\rho_s} \text{ For Solid} \tag{10}$$

$$\overline{P}_w = \frac{1}{2}b_3 h h_w - \frac{\Delta\overline{p}_w h\overline{n}}{\rho_w} \text{ For Fluid} \tag{11}$$

where $\Delta\overline{p}_w$ is the excess pore-water pressure. The interested reader will find in the article by [40] a detailed description of this two-phase SPH model.

Next, the above mathematical equations are completed by using various rheological and empirical laws. In this study, the numerical simulations were performed by using Voellmy's rheological law, which has the same features as the frictional rheological model, and the evolution of pore-water pressure can be considered at the basal surface where the cohesion and all viscous terms are disregarded. The basal shear stress, in the case of a pure frictional mass, is given by

$$\tau_B = -((1-n)(\rho_s - \rho_w)gh - \Delta p_{wb})\frac{\overline{v}_i}{|\overline{v}|}\tan\varphi_b + \rho g\frac{|\overline{v}|}{\xi}\overline{v}_i \tag{12}$$

where τ_B is the basal shear stress, φ_B is the basal friction angle, ξ is the turbulence coefficient, and Δp_{wb} is the excess pore water pressure at the basal surface.

The GeoFlow-SPH code contains various empirical laws governing the landslide growth rate (E_r), such as the Hungr erosion law which is based on an algorithm where the total volume of debris increases by a specified rate, and is given by

$$e_R = E_s \cdot h \cdot \overline{v} \tag{13}$$

where E_s can be obtained directly from the initial and final volumes of the material and the distance traveled as $E_s \approx \ln((V_{\text{final}}/V_0)/(\text{distance}))$.

In the modeling of consolidation, similar to most depth-integrated models, simple shape functions were used to fulfill boundary conditions by assuming that the pore pressure is zero on the free surface and the bottom is impermeable. Consequently, by considering these assumptions, the vertical distribution of pore water pressure can be approximated as

$$\frac{d\Delta p_w}{dt} = -\frac{c_v \pi^2}{4h^2}\Delta p_w \tag{14}$$

where c_v is the consolidation coefficient and h is the mobilized soil depth.

Regarding the time integration scheme, we used the 4th-order Runge–Kutta method, which provides high accuracy in the calculation of ODE. The time step is adaptive and it is calculated progressively under the Courant–Friendrichs–Lewy (CFL) condition.

3. Results

3.1. RAMMS Model

For the terrain model, a pre-event DTM with 5 × 5 m resolution was used. The initial block has an average depth of 15 m, estimated from the analysis of different epoch DTMs. This method was also useful in defining other parameters such as erosion depth (estimated to be a maximum of 20 m in some parts), deposition height, and the outline of debris flow. RAMMS, based on Voellmy rheology, was used to back-calculate parameters of friction and turbulence. After many iterations, the final best-fitted parameters were determined to be 0.11 for friction and 500 m/s^2 for turbulence.

For including entrainment, the default value of 1 kPa was used for critical shear stress, and a rate proportionality factor of dz/dt = 0.1 m/kPa. Greater values of the proportionality factor tend to overpredict erosion volume. The results of volume and transportation of material with and without entrainment were compared. In the case of Selanac, an estimated (on the field) maximum erosion depth of 12 m was used. A comparison of two epochs of DMT was utilized to define the differences in the transportation zone. Considering entrainment, the deposition heights were slightly larger, and the total volume was relatively greater. It can be concluded that entrainment influenced the outflow of material in the Selanačka river, but generally did not change the model of final heights in the deposition zone (Figure 9b,c, Table 3). The model shows a height in the deposition zone of almost 25.56 m, while the final depths in the deposition zone are almost 17 m (Figure 9c).

Table 3. Final results of the parameters in RAMMS model.

Debris Flow	Rheology Model (Voellmy) μ, ξ(ms^{-2})	Volume of Initial Block (m^3)	Volume of Entrainment (m^3)
Selanac	0.11; 500	453,061.15	41,023.35

The other model shows changes in velocity (Figure 9d). The maximum velocity was over 33 m/s, which was also predicted in the Selanačka river zone. However, since we have torrential flow in that zone, this part of the terrain outside the first deposition zone cannot be taken as representative, as velocities in this part were probably much greater due to the river's influence.

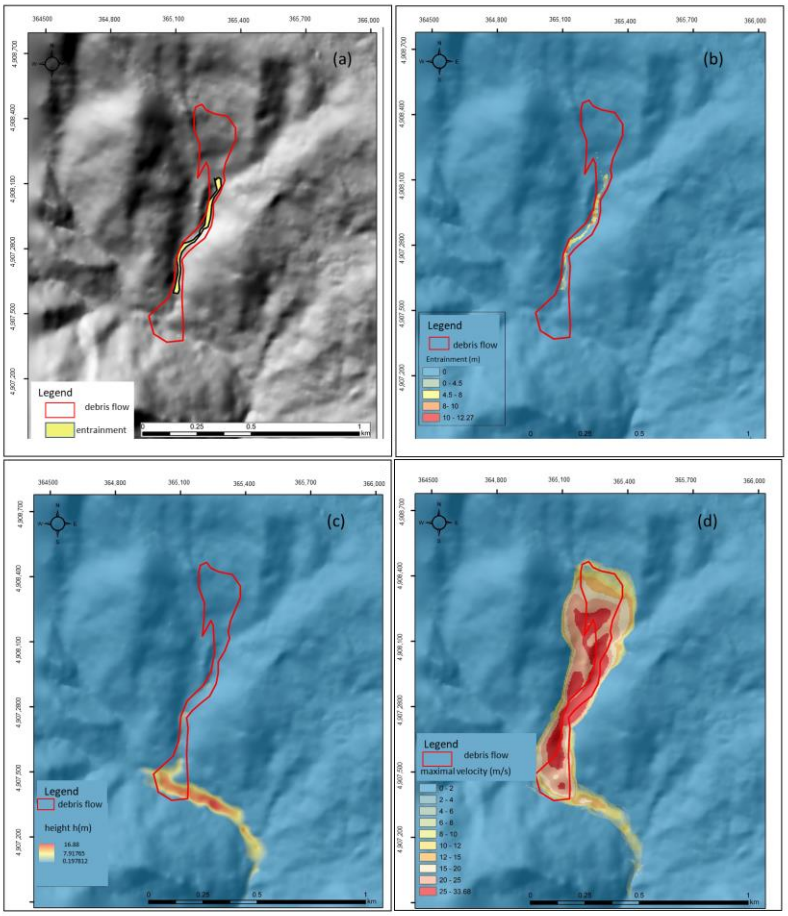

Figure 9. (**a**) Area of entrainment in the transportation zone; (**b**) entrainment model of material in the transportation zone; (**c**) final deposition model; (**d**) maximum flow velocity model of the Selanac debris flow.

3.2. SPH Model

In the SPH code, the same DTM is used as the main topographic file, with representative points totaling 133,452. This results in a substantial number of inputs, which increases the calculation time. The definition of the source area was made in the same way, but here, every point has information about the real depth. The precise definition of the source area is shown in previous work [45]. For the first time, we use the code implementation to subtract the source area from the terrain model, which influences the movement of material. The model is two-phase, including interactions between fluid and soil particles, unlike the previous simplified model.

The selected rheology law is frictional with a Voellmy turbulence coefficient, with $\tan\varphi = 0.35$ (where φ is the frictional angle) and a turbulence coefficient $\xi = 500$ m/s^2. Entrainment influence was defined by the law proposed by Hungr (1995) [1], with the erosion coefficient set to 0.0001. Effects of pore water pressure were not included in this calculation. The final volume of material predicted by this model is 492,300 m^3, while the initial block had a volume of 447,400 m^3, indicating that the amount of material eroded by the action of the fluid is 44,900 m^3. Final models of velocity, entrainment, and final deposition are shown in Figure 10a–d.

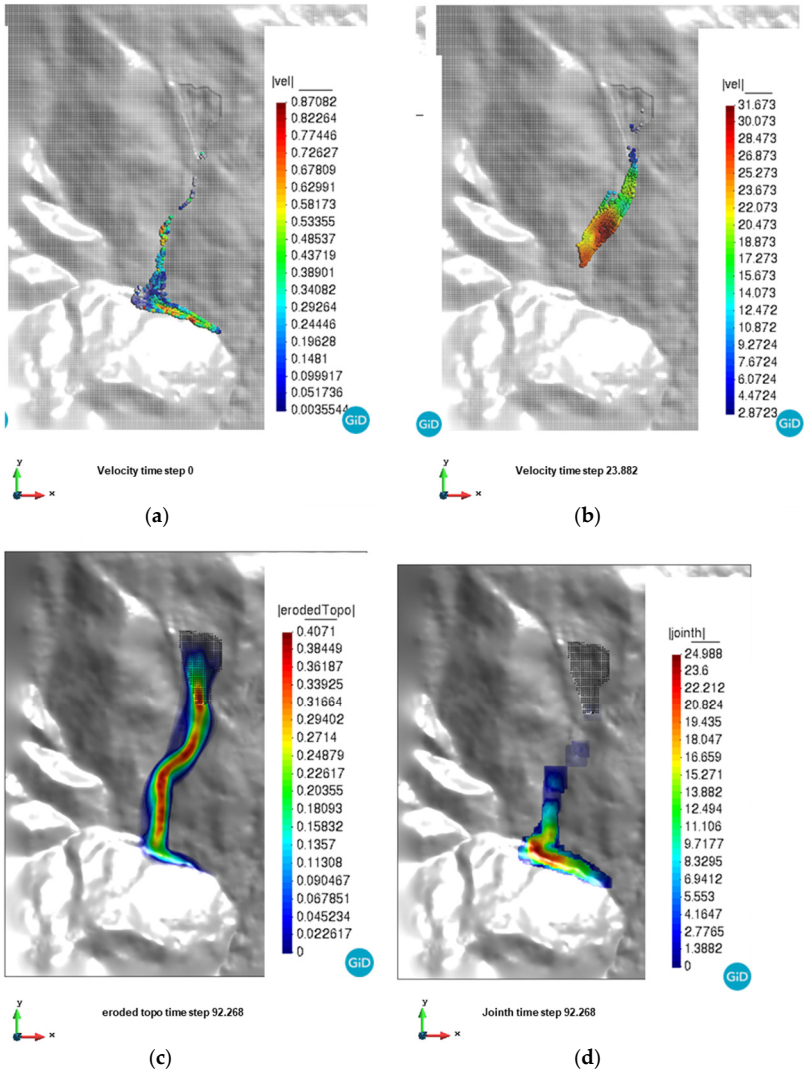

Figure 10. (**a**,**b**) Model for calculating achieved maximum flow velocities; (**c**) model of the material entrainment rate (er); (**d**) model for simulating material movement and final deposition depths.

3.3. Validation

The total motion of material from the main deposition zone further into the Selanačka river valley is also depicted. The final results were compared with deposited material heights measured using ERT (Electric Resistivity Tomography) profiles. According to geophysical ERT investigations, the highest depths of the deposits are about 20 m. As the main profile, we use the same profile position in both the RAMMS and ERT investigations.

Comparison profiles are shown in Figure 11 as well as the final depths in the deposition zone of the SPH models. In both models of final depths, the eroded mass is about 50,000 m^3, which can be concluded from field research, including estimated depths averaging about 10 m. Hence, this amount of material, although not huge in comparison to the total mass, shows an influence in changing depths in the deposition zone in both models.

The maximum velocity registered is about 45 m/s in SPH, while in RAMMS, it is about 33 m/s. Since there are no field measurements during the process, these results are assumed.

The cross-section shows different thicknesses according to the position of the ERT5 profile. For the ERT5 profile, the thickness is shown relative to the lower surface, i.e., the depth of the channel predicted by geophysical investigations (Figure 11). For the models obtained using RAMMS and SPH, the thickness is defined based on the input surface of the DTM. All models predict greater material deposition on the right side of the flow

deposition compared to the ERT5 cross-section. The SPH model predicts greater thicknesses throughout the area but is more representative in the sense that the majority of the material is deposited within the deposition zone. In contrast, the RAMMS model predicts a large amount of overflow material, as seen in the final model (Figure 9c), where the amount of overflow material is significantly greater than the deposited material.

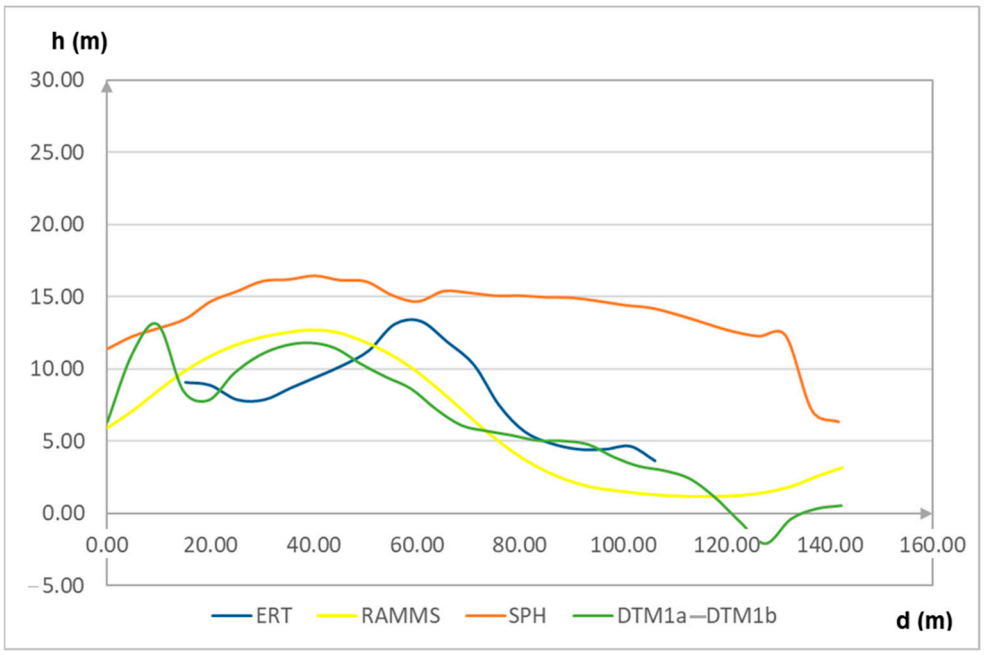

Figure 11. Comparative view of final material depths at position of ERT 5 profile.

The differences in the estimation of deposition depth and calibrated parameters are linked to the distinct solution algorithms on which these two programs are based. The calibration of the turbulence parameter is the same for both flows, while the differences arise in the calibration of the friction parameter. In the case of Selanac, the importance of two-phase flow modeling becomes evident. By using the two-phase SPH model, the deposited material was contained within the deposition zone, unlike in the RAMMS model, where it was not possible to prevent the material from spreading significantly beyond the deposition zone.

4. Conclusions

This research shows the results of the detailed field investigation, with a comparison of two numerical models of the Selanac debris flow. For comparison, different numerical approaches are chosen, one FVM-based (RAMMS DBF program) and the other a meshless method (SPH code). A field investigation was first made using geophysical methods considering how huge debris flows are. Then, a detailed DEM was made to compare two epoch DTMs; the RAMMS model was made continuously for a longer period, in different versions of the program, using different-quality DTMs [43]; the SPH code gives more possibilities in modeling, including different rheology laws. For comparison, here, we use the same constitutive, rheology model. The selected source area is the same, with the possibility to use different depths in SPH since the model is defined in points. For comparison, we used the same position of the profile as profile 5 for ERT investigation (about 20 m).

The Voellmy rheological law was used to ensure the most accurate comparison among the results. The most suitable parameters for the Selanac model were 0.35 and 500 m/s^2, which provide the most realistic representation of material propagation. The validation was performed by comparing a single cross-section, as well as in the case of the RAMMS model, by comparing it with the ERT5 profile and the elevation difference model.

The modeling was significantly more influenced by the prediction of the frictional parameter compared to the turbulence parameter. The final values of the deposited material depth were overestimated in the SPH program compared to the measurements conducted through ERT investigations. On the other hand, the RAMMS model shows a large amount of material flowing through the Selanac River (up to 2/3 of the total material).

The differences in the estimated depth of material deposition and the calibrated parameters are linked to the different solution algorithms on which these two programs are based. The calibration of the turbulence parameter is the same for both flows, while there are differences in the calibration of the friction parameter for both flows. In the case of the Selanac model, the importance of modeling two phases in flows is observed. By using the two-phase SPH model, the deposited material is stopped in the deposition zone, unlike in the RAMMS model, where it was not possible to model the material to prevent it from flowing significantly beyond the deposition zone. These findings indicate that utilizing multiple simulation codes is essential for accurately predicting specific events, evaluating potential risks, and developing appropriate countermeasures.

In the previous study [45,46], various methods were applied to assess the susceptibility to instability in the Ljubovija municipality area. This resulted in susceptibility maps for instability occurrences and a comparison of the accuracy of the applied methods. The Selanac debris flow was activated in areas of mass flow occurrence following extreme rainfall in 2014. The potential for flow development in a broader area, based on defined potential initiation zones and using one of the susceptibility assessment methods, along with rheological parameters established for the Selanac debris flow, provides the possibility to estimate propagation in other potential areas. This could help prevent negative impacts in the future.

Author Contributions: Conceptualization, J.K.; methodology, J.K. and M.P.; software, M.P.; validation, J.K. and S.M.T.; formal analysis, S.M.T. and M.S.-P.; investigation, J.K. and D.Đ.; resources, T.Đ.; data curation, J.K.; writing—original draft preparation, J.K.; writing—review and editing, J.K.; visualization, M.S.-P. and M.M.; supervision, M.P. and B.A.; project administration, B.A.; funding acquisition, B.A. All authors have read and agreed to the published version of the manuscript.

Funding: Field research was part of the project 'BEyond Landslide Awareness' (BEWARE), funded by the People of Japan and the UNDP Office in Serbia (grant no. 00094641). All activities are also part of Project TR36009, funded by the Ministry of Education, Science, and Technological Development of the Republic of Serbia.

Institutional Review Board Statement: Not applicable.

Informed Consent Statement: Not applicable.

Data Availability Statement: The original contributions presented in this study are included in the article; further inquiries can be directed to the corresponding authors.

Acknowledgments: The research results would not have been possible without the ERASMUS+ program between the Polytechnic University of Madrid, Spain, and the University of Belgrade, Serbia. This investigation is included in the PhD dissertation [47].

Conflicts of Interest: The authors declare no conflict of interest.

References

1. Hungr, O. A model for the runout analysis of rapid flow slides, debris flows, and avalanches'. *Can. Geotech. J.* **1995**, *32*, 610–623. [CrossRef]
2. Varnes, D.J. Slope Movement Types and Processes. In *Landslides, Analysis and Control, Transportation Research Board*; Special Report No. 176; Schuster, R.L., Krizek, R.J., Eds.; National Academy of Sciences: Prayagraj, India, 1978; pp. 11–33.
3. Abolmasov, B.; Petrović, M.S.; Stanković, R.; Marjanović, M.; Krušić, J.; Đurić, U. Extreme rainfall event and its aftermath analysis—IPL 210 project progress report. In *Understanding and Reducing Landslide Disaster Risk*; Springer: New York, NY, USA, 2020; pp. 267–273. [CrossRef]
4. Đurić, D.; Mladenović, A.; Pešić-Georgiadis, M.; Marjanović, M.; Abolmasov, B. Using multiresolution and multitemporal satellite data for post-disaster landslide inventory in the Republic of Serbia. *Landslides* **2017**, *14*, 1467–1482. [CrossRef]

5. Rickenmann, D. Empirical Relationships for Debris Flows. *Nat. Hazards* **1999**, *19*, 47–77. [CrossRef]
6. Iverson, R.M. The physics of debris flows. *Rev. Geophys.* **1997**, *35*, 245–296. [CrossRef]
7. Iverson, R.M. Debris flows: Behaviour and hazard assessment. *Geol. Today* **2014**, *30*, 15–20. [CrossRef]
8. Sassa, K. Geotechnical model for the motion of landslides. In Proceedings of the 5th International Symposium on Landslides, "Land-Slides", Balkema, Rotterdam, March 1988; Volume 1, pp. 37–56.
9. Hungr, O.; McDougall, S.; Bovis, M. Entrainment of material by debris flows. In *Debris-Flow Hazards and Related Phenomena*; Springer: Berlin/Heidelberg, Germany, 2005; pp. 135–158.
10. Pastor, M.; Haddad, B.; Sorbino, G.; Cuomo, S.; Drempetic, V. A depth-integrated, coupled SPH model for flow-like landslides and related phenomena. *Int. J. Numer. Anal. Methods Geomech.* **2009**, *33*, 143–172. [CrossRef]
11. Christen, M.; Kowalski, J.; Bartelt, P. RAMMS: Numerical simulation of dense snow avalanches in three-dimensional terrain. *Cold Reg. Sci. Technol.* **2010**, *63*, 1–14. [CrossRef]
12. Pastor, M.; Tayyebi, S.M.; Stickle, M.M.; Yagüe, Á.; Molinos, M.; Navas, P.; Manzanal, D. A depth integrated, coupled, two-phase model for debris flow propagation. *Acta Geotech.* **2021**, *16*, 2409–2433. [CrossRef]
13. Fang, K.; Tang, H.; Li, C.; Su, X.; An, P.; Sun, S. Centrifuge modelling of landslides and landslide hazard mitigation: A review. *Geosci. Front.* **2023**, *14*, 101493. [CrossRef]
14. Frank, F.; McArdell, B.W.; Huggel, C.; Vieli, A. The importance of entrainment and bulking on debris flow runout modeling: Examples from the Swiss Alps. *Nat. Hazards Earth Syst. Sci.* **2015**, *15*, 2569–2583. [CrossRef]
15. Pastor, M.; Tayyebi, S.M.; Hernandez, A.; Gao, L.; Stickle, M.M.; Lin, C. A new two-layer two-phase depth-integrated SPH model implementing dewatering: Application to debris flows. *Comput. Geotech.* **2023**, *153*, 105099. [CrossRef]
16. Tayyebi, S.M.; Pastor, M.; Stickle, M.M. Two-phase SPH numerical study of pore-water pressure effect on debris flows mobility: Yu Tung debris flow. *Comput. Geotech.* **2021**, *132*, 103973. [CrossRef]
17. Bui, H.H.; Fukagawa, R.; Sako, K.; Ohno, S. Lagrangian meshfree particles method (SPH) for large deformation and failure flows of geomaterial using elastic–plastic soil constitutive model. *Int. J. Numer. Anal. Methods Geomech.* **2008**, *32*, 1537–1570. [CrossRef]
18. Bui, H.H.; Nguyen, G.D. Smoothed particle hydrodynamics (SPH) and its applications in geomechanics: From solid fracture to granular behaviour and multiphase flows in porous media. *Comput. Geotech.* **2021**, *138*, 104315. [CrossRef]
19. Bui, H.H.; Sako, K.; Fukagawa, R. Numerical simulation of soil–water interaction using smoothed particle hydrodynamics (SPH) method. *J. Terramech.* **2007**, *44*, 339–346. [CrossRef]
20. Bui, H.; Fukagawa, R.; Sako, K.; Wells, J. Slope stability analysis and discontinuous slope failure simulation by elasto-plastic smoothed particle hydrodynamics (SPH). *Geotech* **2011**, *61*, 565–574. [CrossRef]
21. Akpan, A.E.; Ilori, A.O.; Essien, N.U. Geophysical investigation of Obot Ekpo Landslide site, Cross River State, Nigeria. *J. Afr. Earth Sci.* **2015**, *109*, 154–167. [CrossRef]
22. Rezaei, S.; Shooshpasha, I.; Rezaei, H. Reconstruction of landslide model from ERT, geotechnical, and field data, Nargeschal landslide, Iran. *Bull. Eng. Geol. Environ.* **2018**, *78*, 3223–3237. [CrossRef]
23. Lapenna, V.; Lorenzo, P.; Perrone, A.; Piscitelli, S.; Rizzo, E.; Sdao, F. 2D electrical resistivity imaging of some complex landslides in Lucanian Apennine chain, southern Italy. *Geophysics* **2005**, *70*, B11–B18. [CrossRef]
24. Perrone, A.; Lapenna, V.; Piscitelli, S. Electrical resistivity tomography technique for landslide investigation: A review. *Earth-Science Rev.* **2014**, *135*, 65–82. [CrossRef]
25. Cruden, D.M.; Varnes, D.J. Landslides: Investigation and Mitigation. Chapter 3 Landslide Types and Processes. In *Transportation Research Board Special Report*; Springer: Berlin/Heidelberg, Germany, 1996; p. 247.
26. *ISO 17892-12:2018*; Amd 1:2021: Geotechnical Investigation and Testing–Laboratory Testing of Soil—Part 12: Determination of Liquid and Plastic Limits–Amendment 1. ISO: Geneva, Switzerland, 2018.
27. Frank, F.; McArdell, B.W.; Oggier, N.; Baer, P.; Christen, M.; Vieli, A. Debris-flow modeling at Meretschibach and Bondasca catchments, Switzerland: Sensitivity testing of field-data-based entrainment model. *Nat. Hazards Earth Syst. Sci.* **2017**, *17*, 801–815. [CrossRef]
28. Christen, M.; Bartelt, P.; Kowalski, J. Back calculation of the *In den Arelen* avalanche with RAMMS: Interpretation of model results. *Ann. Glaciol.* **2010**, *51*, 161–168. [CrossRef]
29. Bartelt, P.; Buehler, Y.; Christen, M.; Deubelbeiss, Y.; Graf, C.; McArdell, B.W. *RAMMS–Rapid Mass Movement Simulation, A Modeling System for Debris Flows in Research and Practice, User Manual v1.5, Debris Flow*; Institute for Snow and Avalanche Research SLF: Davos, Switzerland, 2013; p. 126.
30. Lucy, L.B. A numerical approach to the testing of the fission hypothesis. *Astron. J.* **1977**, *82*, 1013. [CrossRef]
31. Gingold, R.A.; Monaghan, J.J. Smoothed particle hydrodynamics: Theory and application to non-spherical stars. *Mon. Not. R. Astron. Soc.* **1977**, *181*, 375–389. [CrossRef]
32. McDougall, S.; Hungr, O. A model for the analysis of rapid landslide motion across three-dimensional terrain. *Can. Geotech. J.* **2004**, *41*, 1084–1097. [CrossRef]
33. McDougall, S. A new continuum dynamic model for the analysis of extremely rapid landslide motion across complex 3D terrain. Ph.D. Dissertation, University of British Columbia, Vancouver, BC, Canada, 2006.
34. Rodriguez-Paz, M.; Bonet, J. A corrected smooth particle hydrodynamics formulation of the shallow-water equations. *Comput. Struct.* **2005**, *83*, 1396–1410. [CrossRef]
35. Li, S.; Liu, W.K. *Meshfree Particle Methods*; Springer: Berlin/Heidelberg, Germany, 2004.

36. Liu, G.R.; Liu, M.B. *Smoothed Particle Hydrodynamics—A Meshfree Particle Method*; World Scientific Publishing Company: Singapore, 2003.
37. Randles, P.; Libersky, L. Smoothed Particle Hydrodynamics: Some recent improvements and applications. *Comput. Methods Appl. Mech. Eng.* **1996**, *139*, 375–408. [CrossRef]
38. Libersky, L.D.; Petschek, A.G. *Smooth Particle Hydrodynamics with Strength of Materials*; Lecture Notes in Physics; Springer: Berlin/Heidelberg, Germany, 2005; pp. 248–257. [CrossRef]
39. Braun, A.; Cuomo, S.; Petrosino, S.; Wang, X.; Zhang, L. Numerical SPH analysis of debris flow run-out and related river damming scenarios for a local case study in SW China. *Landslides* **2017**, *15*, 535–550. [CrossRef]
40. Braun, A.; Wang, X.; Petrosino, S.; Cuomo, S. SPH propagation back-analysis of Baishuihe landslide in south-western China. *Geoenvironmental Disasters* **2017**, *4*, 1–10. [CrossRef]
41. Khairi, M.A.W.; Rozainy, M.R.; Ikhsan, J. Smoothed particle hydrodynamics simulation for debris flow: A review. *AIP Conf. Proc.* **2020**, *2291*, 020093.
42. Zienkiewicz, O.C.; Shiomi, T. Dynamic behaviour of saturated porous media; The generalized Biot formulation and its numerical solution. *Int. J. Numer. Anal. Methods Geomech.* **1984**, *8*, 71–96. [CrossRef]
43. Pitman, E.B.; Le, L. A two-fluid model for avalanche and debris flows. *Philos. Trans. R. Soc. A Math. Phys. Eng. Sci.* **2005**, *363*, 1573–1601. [CrossRef] [PubMed]
44. Pudasaini, S.P. A general two-phase debris flow model. *J. Geophys. Res. Earth Surf.* **2012**, *117*, F03010. [CrossRef]
45. Krušić, J.; Abolmasov, B.; Samardžić-Petrović, M. Influence of DEM resolution on numerical modelling of debris flows in RAMMS—Selanac case study. In *4th Regional Symposium on Landslides in the Adriatic—Balkan Region*; Springer: Berlin/Heidelberg, Germany, 2019.
46. Krušić, J.; Marjanović, M.; Samardžić-Petrović, M.; Abolmasov, B.; Andrejev, K.; Miladinović, A. Comparison of expert, deterministic and Machine Learning approach for landslide susceptibility assessment in Ljubovija Municipality, Serbia. *Geofizika* **2017**, *34*, 251–273. [CrossRef]
47. Krušić, J. The Application of Numerical Methods in Debris Flows Modeling with a Focus on Different Rheological Conditions. Ph.D. Dissertation, University of Belgrade, Belgrade, Serbia, 2024. Available online: https://nardus.mpn.gov.rs/handle/123456789/22758 (accessed on 7 May 2024).